Biochimica et Biophysica Acta 1847 (2015) 153–161

Contents lists available at ScienceDirect

Biochimica et Biophysica Acta

journal homepage: www.elsevier.com/locate/bbabio

Optical identification of the long-wavelength (700–1700 nm) electronic excitations of the native reaction centre, Mn_4CaO_5 cluster and cytochromes of photosystem II in plants and cyanobacteria

Jennifer Morton [a], Fusamichi Akita [b], Yoshiki Nakajima [b], Jian-Ren Shen [b], Elmars Krausz [a,*]

[a] Research School of Chemistry, Australian National University, Canberra, Australia
[b] Photosynthesis Research Center, Graduate School of Natural Science and Technology, Department of Biology, Faculty of Science, Okayama University, Okayama, Japan

ARTICLE INFO

Article history:
Received 5 September 2014
Received in revised form 28 October 2014
Accepted 5 November 2014
Available online 13 November 2014

Keywords:
Photosystem II
Reaction centre
Oxygen evolving centre
Charge-transfer
Circular dichroism
Magnetic circular dichroism

ABSTRACT

Visible/UV absorption in PS II core complexes is dominated by the chl-a absorptions, which extend to ~700 nm. A broad 700–730 nm PS II core complex absorption in spinach has been assigned [1] to a charge transfer excitation between Chl_{D1} and Chl_{D2}. Emission from this state, which peaks at 780 nm, has been seen [2] for both plant and cyanobacterial samples. We show that *Thermosynechococcus vulcanus* PS II core complexes have parallel absorbance in the 700–730 nm region and similar photochemical behaviour to that seen in spinach. This establishes the low energy charge transfer state as intrinsic to the native PS II reaction centre. High-sensitivity MCD measurements made in the 700–1700 nm region reveal additional electronic excitations at ~770 nm and ~1550 nm. The temperature and field dependence of MCD spectra establish that the system peaking near 1550 nm is a heme-to-Fe(III) charge transfer excitation. These transitions have not previously been observed for cyt b_{559} or cyt c_{550}. The distinctive characteristics of the MCD signals seen at 770 nm allow us to assign absorption in this region to a $d_z^2 \rightarrow d_{x2-y2}$ transition of Mn(III) in the Ca-Mn_4O_5 cluster of the oxygen evolving centre. Current measurements were performed in the S_1 state. Detailed analyses of this spectral region, especially in higher S states, promise to provide a new window on models of water oxidation.

1. Introduction

PS II core complexes are widely utilised to study the spectroscopy as well as the fundamental photo-physics and photochemistry occurring in PS II. These complexes are the minimal photosynthetic assemblies capable of evolving oxygen. PS II cores incorporate CP43 and CP47 proximal antennae, these being intimately attached to its D1/D2/cyt b_{559} reaction centre protein assembly. Isolated D1/D2/cyt b_{559} reaction centre assemblies [3] undergo charge separation but do not bind plastoquinones and their tyrosines are not photoactive. Additionally, they do not retain the OEC containing the catalytically active Mn_4CaO_5 cluster. We have demonstrated [4] that the reaction centre present in PS II core complexes of spinach differs from that of isolated D1/D2/cyt b_{559} in their spectral characteristics, particularly in the 700–730 nm range. There is no equivalent absorption in the D1/D2/cyt b_{559} assemblies in the 700–730 nm region to that seen in spinach core complexes.

PS II core complexes can be prepared to have an oxygen-evolving capacity approaching that of membrane bound PS II and thylakoids. Core complexes isolated from *Thermosynechococcus vulcanus* (*T. vulcanus*) and closely related thermophiles have been successfully crystallised, allowing a crystal structure determination [5] to atomic resolution (1.9 Å). These crystal structures have been a strong impetus to both theoretical and experimental studies; a primary goal being the determination of the mechanism of catalytic water oxidation.

It has long been known that illumination of PS II in the 700–900 nm region gives rise to significant changes in Mn_4CaO_5 related EPR spectra [6,7]. These effects are dependent on the S state being measured and the sequence/temperature whereby near-IR illumination is utilised. The Mn_4CaO_5 based absorption responsible for this photo-activity is thought [7] to be either a d–d transition within Mn(III) d^4 configuration(s) or a charge transfer (mixed valence) absorption(s) of neighbouring Mn(III)–Mn(IV) pair(s). Resonance Raman spectroscopy [8] has also been used to provide evidence for an Mn-based absorption in the 800 nm region.

There were early reports [9,10] of transient absorption changes exhibited in the 700–900 nm range in experiments on PS II membrane preparations following flash illumination. These changes were of the magnitude of $\Delta\varepsilon$ ~100 M^{-1} cm^{-1} but showed no distinct spectral features. An attempt [11] was made to monitor changes in the near-IR absorption of concentrated preparations of highly oxygen-evolving

Abbreviations: PSII, photosystem II; OEC, oxygen evolving centre; Near-IR, near infrared; CD, circular dichroism; MCD, magnetic circular dichroism; EPR, electron paramagnetic resonance; UV/Vis, ultra violet/visible; LMCT, ligand to metal charge transfer; DRS, deep red state; Chl-a, chloropyll-a

* Corresponding author. Fax: + 61 2 6125 0750.
E-mail address: elmars.krausz@anu.edu.au (E. Krausz).

http://dx.doi.org/10.1016/j.bbabio.2014.11.003
0005-2728/

spinach PS II cores, following intense 5 ns 532 nm YAG laser flashes at 0 °C. These flashes transiently created the $S_2Q_A^-$ configuration of PS II from the (resting) S_1Q_A state, the former having a lifetime of ~60 s at 0 °C in spinach. Flash induced transmission changes were measured, a single wavelength at a time. This allowed a broad near-IR difference spectrum, peaking near 800 nm to be accumulated, having $\Delta\varepsilon$ ~100 M^{-1} cm^{-1}. The spectral profile of this transient absorption change matched the EPR action spectra reasonably well and the phenomenon was attributed to an oxidation process within the Mn_4CaO_5 cluster, and associated with the S_1 to S_2 step. However, using a CCD spectrometer [12] to later repeat this experiment, this transient absorption feature was seen to be due to the creation of a small concentration (1 mol%) of the radical $P680^+$. The long-lived $S_1(P680^+)Q_A^-$ species appears to be in thermodynamic equilibrium with the $S_2Q_A^-$ state, indicating an ~110 mV electrochemical difference between the $S_1(P680^+)Q_A^-$ and $S_2Q_A^-$ configurations in spinach cores.

So as to provide direct optical signature(s) for the Mn_4CaO_5 based absorptions responsible for the well-known EPR changes induced by long wavelength illumination, we have explored the near-IR spectral region in detail, using low-temperature absorption, CD and MCD techniques. The MCD technique in particular, can be expected to show distinctive behaviour for Mn(III)-based Mn_4CaO_5 excitations. Although absorption in the near-IR is weak, Mn_4CaO_5 based excitations potentially have a (relatively) strong MCD signal. The magnetic field dependence as well as temperature dependence of the MCD signal is different for the various chromophores present in the near-IR region. For chlorophylls and other diamagnetic species, MCD *B* terms are present. *B* terms [13] are temperature independent, and have the same shape as the absorption giving rise to the dichroism and have amplitudes that are linear in the applied magnetic field.

For odd-electron paramagnetic species, such as oxidised cytochromes, an MCD *C* term [13] is dominant at low temperatures. An MCD *C* term for a g ~2 system typically has a 1/temperature dependence above ~10 K but becomes strongly saturated when approaching ~2 K in a 5 T applied magnetic field. For even-electron paramagnets such as high-spin Mn(III) or Fe(II) species, complex MCD signatures can be expected to occur. This complexity is due to the magnetic field induced mixing and shifting of the manifold of spin-orbit levels of the ground state configuration. Even electron paramagnet-based MCD signals are characteristically much stronger (relative to absorption) than 'normal' *B* terms and have distinctive field and temperature dependences [14] in the 1.5–40 K range.

There have been a number of studies of Mn(III) catalase μ-oxo dimers [15,16] and related model compounds [17], as well as Mn(III) monomers [18] that highlight the capacity of MCD to help identify the detailed coordination and geometry of these systems.

The molar extinction of lowest-energy Mn(III) excitations is characteristically low [11] and in the range of 10–100 M^{-1} cm^{-1}. This places them as ~1000× weaker than chlorophyll Q_y absorptions in the visible region. The Mn(III) MCD induced by a 5 T magnetic field is however, relatively strong, with $\varepsilon_L - \varepsilon_R$ of ~0.1–5 M^{-1} cm^{-1} having been reported [17]. The *B* term MCD of chl-a in the Q_y region using an applied field of 5 T has a value of [19] $\varepsilon_L - \varepsilon_R$ ~160 M^{-1} cm^{-1}. The relative MCD, $\varepsilon_L - \varepsilon_R$ / ε or equivalently $A_L - A_R$ / A, may be as high as ~0.1 for Mn(III) excitations but has a value of only ~0.002 for Q_y excitations of chl-a in an applied field of 5 T.

Low-spin ferric cytochromes are known to exhibit a strong *C* term MCD signal in the near-IR, peaking in the 1300–1700 nm region. This band system has been assigned to a heme-to-Fe(III) LMCT process. An excellent review of MCD in hemoproteins is provided by Cheesman and Thomson [20]. The MCD *C* term $\varepsilon_L - \varepsilon_R$ value in an applied magnetic field of 5 T can be relatively strong, having $\varepsilon_L - \varepsilon_R$ of ~300 M^{-1} cm^{-1}. The position and MCD saturation behaviour [21] of this band can be used to characterise the detailed coordination of the cytochrome responsible for the absorption and provide complementary information to EPR data. Although the ~1600 nm range is well outside our primary area of interest, the broad LMCT cytochrome band system extends to ~800 nm. The low-temperature MCD peak $\varepsilon_L - \varepsilon_R$ of this band is ~100× stronger than that expected for Mn(III) and thus residual MCD intensity of this band near 800 nm may be significant.

In a previous paper [2] we have investigated the characteristic PS I content of PS II core complex preparations in detail. We developed a fluorescence procedure whereby such contamination could be quantified. Although it was possible to identify PS II core complexes isolated from winter-grown spinach that had no measureable PS I content, PS II prepared from *T. vulcanus*, even those from recrystallised preparations, showed some residual PS I content. An additional caveat was that the precise spectral profile of the PS I species present in any specific PS II preparation could vary [2].

The main aim of this paper is to help identify potential Mn_4CaO_5 based absorption(s) in the near-IR region. This necessitates a careful monitoring of potential overlap of Mn(III)-based transitions with other absorptions in the near IR. The 700–730 nm DRS in the PS II reaction centre in spinach cores has been established [1] to have a $\varepsilon = 8000$ M^{-1} cm^{-1} at 705 nm. The DRS has no measureable CD and has [22] a 5 T *B* term MCD at 705 nm of $\varepsilon_L - \varepsilon_R$ ~10 M^{-1} cm^{-1}. This MCD signal is then of similar magnitude to that anticipated for Mn(III) transitions at low temperatures. Ferric cytochrome MCD signals at 1.6 K and 5 T exhibit a $\varepsilon_L - \varepsilon_R$ of the order of 300 M^{-1} cm^{-1} at ~1600 nm. The corresponding $\varepsilon_L - \varepsilon_R$ value in the 800–900 nm region may well have a similar MCD magnitude to that of the DRS (700–730 nm) and that of Mn(III) (700–900 nm).

The ε value of PS I at 710 nm is ~10^6 M^{-1} cm^{-1}, with PS I 'red trap' Q_y absorptions extending to ~740 nm in both spinach and *T. vulcanus*. Assuming a PS I contamination level of ~1 mol% of PS I in a PS II core sample, the PS I contribution to absorption at 710 nm would then have an apparent ε of ~10,000 M^{-1} cm^{-1}. The Q_y *B* term MCD at 5 T from this contamination could then be expected to have an apparent Q_y $\varepsilon_L - \varepsilon_R$ of ~20 M^{-1} cm^{-1}. This is again of the same magnitude in low-temperature MCD as the other chromophores in the 700–900 nm spectral region. Fortunately the PS I 'red trap' has a strong and distinctive CD spectrum, which helps to distinguish it from the PS II based DRS absorption in the same spectral region.

2. Materials and methods

Absorption, CD and MCD spectra were all measured simultaneously on a dedicated laboratory-constructed spectrometer, based on a Spex 0.75 M monochromator. This system has been previously described [23,24]. Gratings blazed at 200 nm, 500 nm and 1000 nm were utilised in the UV, visible and near-IR regions. End-window photomultipliers were used in the visible spectral range with measurements in the 750–1100 nm region being made with a windowless, 5 mm ϕ Advanced Photonix silicon avalanche diode. The very high quantum efficiency and low noise of this latter detector have enabled a large increase in MCD sensitivity of the spectrometer in the near-IR 700–1000 nm region. A 1 mm, liquid nitrogen cooled InSb detector system, together with condensing optics, was used in the 800–2000 nm range. The spectral source in the UV/Vis was a laser driven light source and that in the visible/near-IR region being a highly stabilised 240 W halogen lamp.

A Ti:S laser (Schwartz EO) pumped with a Continuum Verdi G CW laser operating at 532 nm was used as a near-IR excitation source. Other critical details regarding the laser light purity and illumination/sample protocols were as previously described [1]. The construction of the strain-free fused quartz sample cells utilised has been described previously [25,24].

The PS I and PS II samples used in this work were also the same or very similar to those recently used [2] to measure the 780 nm emission from the DRS. The oxygen evolving capacity of the non-recrystallised preparations is typically 3000 μmol of O_2 $(mg\ chl)^{-1}$ h^{-1} and EPR multiline signals are readily obtained from the samples [26,27]. Both

these measurements are indicative of an intact and functional OEC. Multiline S_2 EPR spectra have also been obtained from single crystals [28].

So as to provide samples with high optical transmission, PS I and PS II preparations were diluted with ~40% (v/v) of a 1:1 (v/v) mixture of ethylene glycol and glycerol which was performed immediately before glassing of the sample to liquid helium temperatures over a period of 2 min. The optical characteristics of samples were checked by monitoring the CD spectrum of a solution containing an optically active material, when placed in the spectrometer beam and in a position where light had already passed through the low-temperature sample. Typically, no change in the CD spectrum of optically active material occurred, establishing the optical integrity of the low-temperature sample.

3. Results

3.1. Illumination dependent spectra of PS II and PS I

Low-temperature (<77 K) visible absorption spectra of PS II cores are strongly influenced by deliberate and/or accidental illumination and also by actinic (measurement) light. Specifically, following absorption by any chromophore that gives rise to excitation transfer to the PS II reaction centre, the secondary acceptor Q_A becomes photo-reduced to form the metastable Q_A^- anion. Such, photo-reduction is evidenced by an electrochromic shift of the $Pheo_{D1}$ Q_x band near 550 nm (the C550 shift [29]) along with a concomitant oxidation of either a (reduced) cyt b_{559} when available, or by the creation of another secondary donor such as an oxidised chl-a or β-carotene. The quantum efficiency of low-temperature metastable photo-reduction of Q_A approaches unity for a significant fraction of the PS II complexes [1]. The C550 shift can be used to quantify illumination-induced photo-reduction of the sample, as is exampled in Fig. 1 of Hughes et al. [1]. The $CaMn_4O_5$ cluster is not available as an electron donor at low temperatures.

As CD and MCD spectroscopy involves the measurement of very small ($A_L - A_R$ ~10^{-3}–10^{-6}) circular polarisation dependent differences in absorption and these measurements inevitably lead to the sample accumulating a significant actinic response [24]. This accumulated actinic load will induce significant photo-reduction of Q_A with concomitant secondary donor formation whenever measurements are made in a spectral region that leads to excitation of the PS II reaction centre. The Q_A photo-reduction process becomes progressively less efficient [1] with longer wavelength illumination in the 700–730 nm region but remains a consideration.

We have previously established [1] a protocol which allows for the measurement of low temperature PS II absorption spectra with minimal actinic change of the sample. This involves the use of defocused measurement light, 12 mm diameter samples with low light scattering properties, 50 μ spectrometer slits and relatively rapid spectral scans. A comparison of sequential absorption spectra measured in this way exhibits minimal differences, corresponding to less than 1% photoconversion of all Q_A to Q_A^- in a single scan.

Fig. 1 provides an overview of the UV/Vis (non-actinic) absorption of a highly concentrated PS II preparation of *T. vulcanus*, taken at 1.6 K, measured in both a thin (25 μm) and thick (1 mm) path-length quartz cells. Spectra were taken with the PS II sample poised in the S_1-Q_A state, via a 20 min dark adaption at room temperature, followed by rapid freezing. Care was taken to ensure that the samples received no illumination in the 200–730 nm region before measurements were made. If necessary, samples were viewed with night vision goggles whilst using 800 nm light.

Absorption spectra of the C550 region are only just feasible with our thick sample, the minimum absorption (occurring at 552 nm) being ~4. The optical density of the sample at the commonly used excitation wavelength of 532 nm is 4.6 and the extrapolated value at the 514 nm Ar^+ laser line is 11.1. The extrapolated optical density at the peak of the Q_y (675 nm) is 44. Illumination of such an optically dense sample with visible light leads to the interior of the sample receiving many orders of magnitude less light than the side facing the incident light source.

Our ability to measure accurate absorption spectra of a thick, concentrated PS II sample having an optical density in the range from 4 to 5 in the 550 nm region may appear surprising. The normal maximum for measureable optical densities is in the range of ~2–3 for most samples, due to stray polychromatic light in the spectrometer. However, a concentrated PS II sample is extremely opaque nearly throughout the entire UV/Vis region and acts as its own stray light filter for measurements in the 550 nm window. By using a high sensitivity detector and the dynamic range available with a lock-in amplifier and the single beam approach [30], accurate measurements can be made up to an optical density of 5. This was confirmed by comparing corresponding spectra of the same preparation taken on samples 5 times thinner.

The 710 nm absorption feature evident in the spectra in Fig. 1 indicates that the PS II sample contains PS I. We had previously determined the PS I content of similar PS II preparations to be ~0.6 mol%, using a fluorescence method [2]. This PS I absorption serves to mask DRS absorption of PS II.

PS I has a strong and distinctive CD spectrum in the 700–740 nm region. Fig. 2 provides simultaneously-recorded reference absorption, CD and MCD spectra of purified PS I of *T. vulcanus* taken at 1.6 K. The absorption spectrum is in good agreement with that previously published [31] for the closely related organism *Thermosynechococcus elongatus*.

By comparing the calibrated CD spectra of purified PS I (see Fig. 2), to absorption and CD spectra of the PS II sample used in Fig. 1, the concentration of PS I in this preparation can be determined as 1.6 mol%. This PS I concentration is somewhat higher than the value in a similar non-recrystallised preparation used previously, which was 0.6%. This overall level of PS I concentration was confirmed by utilising the fluorescence method [2] and is an inherent feature of these preparations.

The CD spectra in the 700–740 nm range of the purified PS I sample and the PS II sample have the same distinctive spectral profile,

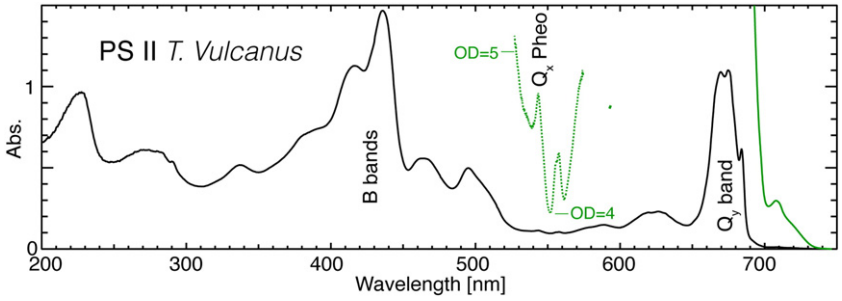

Fig. 1. Non-actinic overview absorption spectra of ~10 mg/ml PS II preparation (60%v/v) containing 1.6 mol% PSI in 40% v/v 1:1 ethylene glycol:glycerol cryoprotectant at 1.6 K. Pathlengths were 1 mm (green) and 25 μm (black).

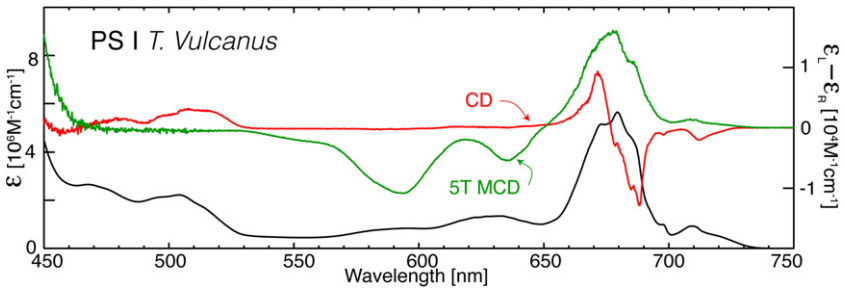

Fig. 2. Calibrated absorption, CD and 5 T MCD spectra of PS I prepared of *T. vulcanus* at 1.6 K.

establishing that any PS II based CD in this region is indeed small. This is entirely consistent with the fact that for spinach preparations containing <0.05 mol% PS I, the 700–730 region has no observable CD. In the cyanobacterial sample, subtraction of PS I based absorption, as determined from the amplitude of the characteristic PSI, from spectra of PS II preparation containing 1.6% PS I, allows the residual DRS PS II absorption in the 700–730 nm region to be determined. Fig. 3 shows that *T. vulcanus* PS II exhibits a DRS red tail, with ε ~8000 M^{-1} cm^{-1} at ~703 nm. The feature is very similar to that reported for spinach PS II [1]. The (positive) CD remaining after the PS I component is subtracted peaks near 682 nm associated with the proximal antenna CP47. We were not able to observe any CD attributable to the DRS.

The MCD of the DRS can also be determined by subtraction of that MCD component due to PS I. The DRS has positive *B* term MCD with $\varepsilon_L - \varepsilon_R$ ~18 M^{-1} cm^{-1} at 703 nm and 5 T, analogous to that seen for spinach PS II [22].

Only relatively small amounts of recrystallised PS II from *T. vulcanus* are available. As noted previously [2], the recrystallised material has far less PS I, but the residual PS 1 particles present have different spectral characteristics to that of purified PS I as seen in Fig. 2. By contrast, the PS I present in the non-recrystallised PS II preparation appears to be essentially identical in emission, absorption, CD and MCD characteristics to that of our purified PS I. Quantitative correction for contamination with well defined PS I in non-recrystallised PS II preparations has the significant advantage that the non-recrystallised material can be more highly concentrated, has less optical scatter and is available in the volumes needed for high sensitivity MCD measurements in the near-IR region.

As well as retaining a significant amount of PS I and perhaps other proteins with variable spectral characteristics, we have found that recrystallised PS II samples exhibit some minor spectral characteristics that differ to those of the non-recrystallised material. The Supplementary data (Fig. S1A) show that the cyt b_{559} present is approximately 80% oxidised compared to the non-recrystallised material. In this way the recrystallised *T. vulcanus* core complexes resemble spinach core complexes, in which the cyt b_{559} is fully oxidised. Except for relatively minor details, the recrystallised cores were found to perform the same overall photo-reduction and other processes and exhibit the same spectral features as seen in the non-recrystallised preparation.

Using the CD calibration of the PS I content outlined above, the absorption spectrum of the un-recrystallised material can be quantitatively corrected for the PS I content (Fig. 3). When this correction is made and the spectrum compared to that of recrystallised PS II samples, their absorption profiles can differ markedly in the Q_y region, especially around 690 nm (Fig. S1B). The increased absorption in the long wavelength spectral region seen for one recrystallised sample (b) is likely to be responsible for the unexplained tailing emission previously observed in this particular PS II sample [2]. Illumination experiments (see Supplementary information) establish that absorption changes in recrystallised sample (b) are not entirely related to the DRS. Overall, measurements on the non-recrystallized PS II preparation, once corrected for PS I content, were found to provide the most consistent results.

The DRS red tail in spinach PS II exhibits a 40% drop in absorption intensity upon photo-reduction of Q_A^- associated with low-temperature illumination [32]. This phenomenon is also observed in *T. vulcanus*. Direct excitation into the DRS in the 700–730 nm region leads to photo-reduction of Q_A. In spinach PS II, a ~45% conversion to the Q_A^- was achieved by absorption of ~1 J/cm^2 at 720 nm (Fig. 1 of [1]). Fig. 4 reproduces this result for *T. vulcanus*. The main difference is that in *T. vulcanus* the (reduced) cyt b_{559} serves as a preferred secondary donor, leading to the bleach feature at 557 nm.

The Supplementary information (Fig. S3A, B and accompanying text) explores PS I based near-IR absorption and MCD as well as low temperature illumination-induced absorption changes of PS I when using the same illumination protocols as utilised for PS II samples. In the 690–850 nm region, absorption and MCD due to $P700^+$ near 810 nm is quantified. These data establish that illumination-induced absorption changes seen for the 700–730 nm region are associated with the DRS of PS II and are not associated with any PS I content of the non-recrystallised PS II preparation (Fig. 3).

3.2. Near-IR absorption and MCD

In the previous section we established that *T. vulcanus* exhibits a DRS in the 700–730 nm region having properties that are analogous to those seen for spinach. As discussed above, high-sensitivity MCD measurements at wavelengths shorter than 730 nm may be affected by

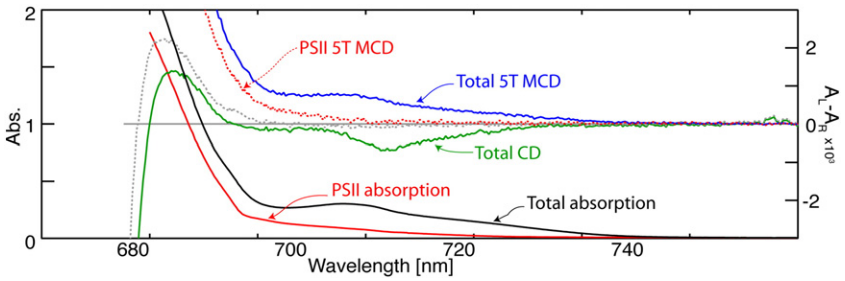

Fig. 3. Far-red absorption, CD and MCD spectra at 1.6 K of the *T. vulcanus* PS II preparation used in Fig. 1. Also shown is the absorption, CD and MCD component due purely to PS II once the PS I absorption, as scaled by the strong CD feature at 710 nm (Fig. 2), has been subtracted.

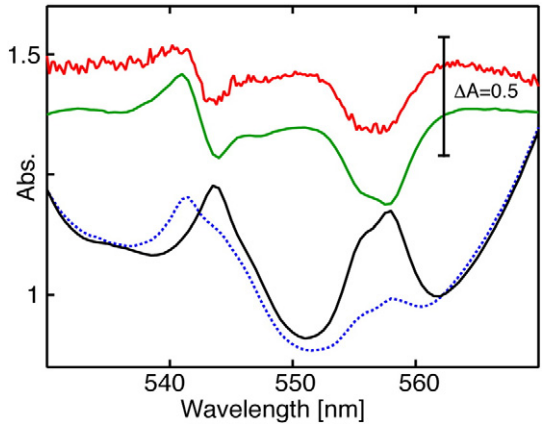

Fig. 4. The blue and black traces are absorption spectra at 1.6 K of the concentrated, non-recrystallised (~6 mgs/ml after dilution with 1:1 (v) ethylene glycol/glycerol) *T. vulcanus* PS II sample in a 200 μm pathlength cell, before and after illumination with broadband green light, leading to >90% photoreduction of Q_A. The green trace is the difference spectrum displaying the characteristic C550 shift. Analogous results have been published for *T. elongatus* [34]. The red trace is the corresponding difference spectrum after laser illumination at 720 nm in a 1 mm pathlength cell. The difference is scaled by the relative path-length of the two cells. The absorbed fluence by the DRS of PS II was ~1 J/cm^2. The ~50% photoconversion seen using 720 nm light reproduces the corresponding experiment in spinach, as seen in Fig. 1 of ref [1].

measurement light. Specifically, photo-reduction of Q_A leads to reduced DRS absorption and its related MCD in the 700–730 nm region. Each spectral scan would then serve to accumulate changes in absorption and MCD spectra, prohibiting accurate measurements.

In Fig. 5 we show high-sensitivity, field and temperature dependent MCD spectra of the dark-adapted, 1 mm thick PS II sample seen in Fig. 1, for the 730–900 nm region. Care was taken to avoid illumination at wavelengths greater than 730 nm. The visible spectrum (Fig. 1) was taken with very low incident light levels, so as to eliminate actinic effects.

Each MCD trace in Figs. 5 and 6 was determined by recording a spectrum with an applied field of 5 T and then subtracting the corresponding spectrum recorded with a −5 T applied field and subsequent division by 2. This procedure removes baseline effects that are associated with the intrinsic polarisation response seen whenever a semiconductor diode is utilised as a MCD detector. Semiconductor detectors have the advantage of being not significantly influenced by stray magnetic fields, as are photomultipliers.

We have found that MCD spectra taken from differing samples at different times were entirely reproducible, with the caveat being that small ($A_L - A_R$ ~1–5 × 10^{-5}) but unpredictable offsets of the entire MCD spectrum occurred. These offsets were due to microscopic movements of the sample, relative to the measurement beam. These movements arose when the superconducting magnet was either energised or de-energised. Analogous offsets could be introduced by making very small but deliberate translations of the sample/magnet-cryostat relative to the measurement beam.

The presence of minute offsets of this nature would normally not be a problem in MCD spectroscopy, as it would suffice to refer to a spectral region having no MCD signal and simply calibrate the various offsets at this point. The difficulty in the current case is, from the temperature and field dependent data seen in Fig. 5, there is no region in the entire range that does not exhibit an MCD signal.

A detailed comparison of all the field and temperature dependent spectra in the 860–900 nm region for a given sample establishes that MCD spectra maintain the same spectral shape in this region. This indicates that the MCD in the 860–900 nm region is dominated by cytochrome LMCT transitions (see introduction Fig. 7). Thus the relative amplitudes of cytochrome-related MCD spectra can be determined, via the multiplicative factor connecting the common spectral feature (in our case a rising tail). This procedure leaves only a single undetermined offset parameter.

A comparison of the relative amplitudes of the 860–900 nm MCD recorded at various fields and temperatures with the saturation curve of a cytochrome-c oxidase which exhibits an LMCT band at 1564 nm [33], show good agreement. We can then use the cytochrome-c oxidase saturation curve [33] to estimate the remaining offset parameter. This leads to the offset-corrected spectra shown in Figs. 5 and 6.

The temperature dependence and field dependence seen in Fig. 5 identify the positive-going and temperature independent MCD feature, also prominent in absorption spectrum of the 730–740 nm region, to be a MCD *B* term. From its sign and magnitude and by referral the PS I MCD spectra in Fig. 2, this component can be attributed to the PS I present in the sample. There is PS I-based near-IR absorption and MCD associated with $P700^+$ at 810 nm (Supplementary Information Fig. S2A, B). However, these signals are very weak and do not contribute significantly to the MCD seen in Fig. 5.

The MCD in the 860–900 nm region shows reciprocal absolute temperature dependence (i.e. varies as 1/Temperature) above 10 K and has strong saturation behaviour at 1.6 K when approaching an applied magnetic field of 5 T. As discussed in Section 1 Introduction, oxidised cytochromes have a broad charge transfer band peaking near 1600 nm which exhibits such MCD *C* term behaviour [20].

The r.h. panel of Fig. 6 shows the low-temperature MCD, in the 800–1800 nm region, of a spinach PS II core sample. Spinach cores have cyt b_{559} fully oxidised and the MCD seen peaking at 1530 nm, is very similar to other oxidised low-spin cytochromes [20]. The l.h. panel of Fig. 6 shows the 730–900 nm temperature dependent MCD. The scale used in this figure, relative to Fig. 5, compensates for the fact that the spinach sample is approximately 2.5 times less concentrated than that for *T. vulcanus*. The *B* term behaviour of residual PS I is evident,

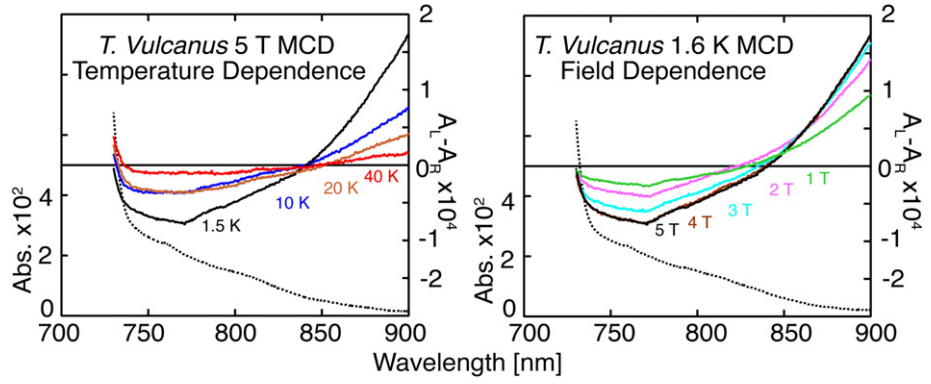

Fig. 5. The temperature and field dependent MCD (r.h. scales) of the ~6 mg/ml, 1 mm thick *T. vulcanus* PS II sample reported in Fig. 1 are presented above at the temperatures and field indicated. Each MCD spectrum is the average of spectra taken positive and negative applied fields and offsets have been adjusted (see text). The sample was dark adapted for 20 min to relax to the S_1 state and subsequently not illuminated at wavelengths less than 730 nm. The absorption spectrum (l.h. scales) is the dotted line.

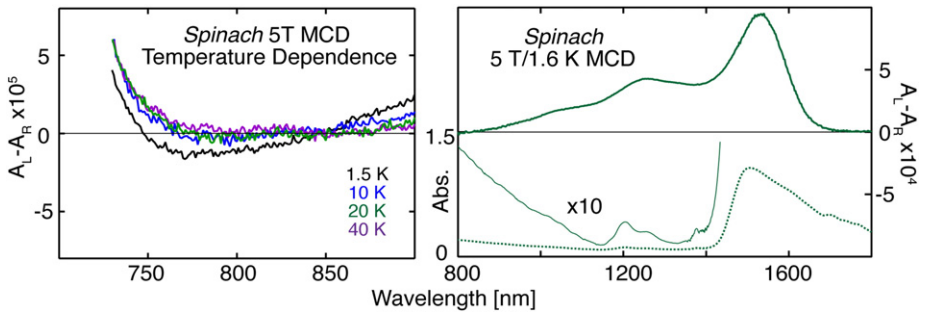

Fig. 6. The left hand panel shows temperature dependent MCD spectra of a ~2.4 mg/ml chl-a PS II sample of spinach containing ~2 mol% PS I in a 1 mm path-length cell. The corresponding absorption trace was featureless and is not presented. The r.h. panel shows absorption (l.h. scale) and MCD (r.h. scale) at 5 T and 1.6 K extended to the 800–1600 nm region. Each MCD spectrum is the generated by subtracting spectra taken at 5 T and -5 T.

extending to ~760 nm for this PS II spinach sample. Temperature dependent MCD is seen near ~770 nm, but signal-to-noise suffers from lower the lower signal strength of a more dilute sample (see above). The positive MCD *C* term behaviour near 900 nm is similar to that seen in *T. vulcanus* (Fig. 5), albeit weaker.

T. vulcanus has *two* low-spin cytochromes; cyt c_{550} and cyt b_{559}. In the native state, cytc_{550} is oxidised and cytb_{559} reduced. In preparing PS II core complexes, a fraction of cyt b_{559} can become oxidised. Furthermore, cyt b_{559} can be easily photo-oxidised at low temperatures (Fig. 4). Fig. 7 shows the long-wavelength absorption and MCD of a *T. vulcanus* sample having a large fraction of the cyt b_{559} reduced. The second panel of Fig. 6 shows the characteristic MCD *C* term temperature dependence of oxidised low-spin cytochromes seen in the 800–1800 nm region. This band arises largely from cyt c_{550}, as cyt b_{559} is mostly reduced in the non-illuminated sample.

Supplementary information (Fig. S3 and related text) examines absorption and MCD near-IR spectral changes upon low temperature illumination of the sample, leading to cyt b_{559} photo-oxidation. Difference spectra provide the MCD of photo-oxidised cyt b_{559}. Estimates of its absorption are also provided. These spectra also show absorption near 980 nm due to the creation of a small amount of β-carotene^{+} via the illumination.

The MCD of cyt c_{550} (Fig. 7) peaks at 1535 nm and is somewhat narrower (~90 nm FWHM) than the cyt b_{559} 1530 nm peak of spinach with FWHM of ~130 nm (Fig. 6). The MCD of photo-oxidised of cyt b_{559} in *T. vulcanus* (Fig. S3) peaks at 1525 nm and is also narrow with FWHM ~70 nm.

Significantly, the cytochrome-based MCD spectra in Fig. 7 all extend to ~830 nm. They exhibit well-defined, *C* term (reciprocal) temperature dependence. This is in contrast to the more complex temperature and field dependent MCD spectra in the 730–800 nm region (Figs. 5, 6). The MCD feature at 770 nm reduces in magnitude more rapidly with increasing temperature than the dominantly cytochrome tail in the 860–900 nm region. There are also indications of another band system near 800 nm in Fig. 5, having field and temperature dependences somewhat different to that for the 770 or 900 nm regions. Spectra taken from spinach PS II (Fig. 6) are analogous but less distinct in the 750–900 nm region, due to ~2.5× lower sample PS II concentration here and somewhat poorer optical quality of this sample.

Weak absorption features appear at ~760 nm and ~800 nm (Fig. 4). These features are not evident in spectra of samples containing cryoprotectant and buffer only. They are assigned as vibrational overtones associated with the protein. Similar features are seen in concentrated PS I samples and are thus are not specific to PS II. There appears to be no absorption feature corresponding to the (negative) MCD peaking at 770 nm. A more detailed examination of the absorption in this spectral region (Supplementary information Fig. S4) allows us to estimate an upper limit to the molar extinction of any underlying Mn(III) absorption near 770 nm to be $<30\ M^{-1}\ cm^{-1}$.

4. Discussion

4.1. The deep red state (DRS)

We have been able to show that the DRS, as evidenced by absorption in the 700–730 nm region, has very similar properties in *T. vulcanus* as to that seen in spinach. It has been previously reported [34] that long wavelength illumination of *T. elongatus* PS II samples did lead to charge separation and subsequent Q_A^- formation but a quantification of the process requires a DRS absorption spectrum. The DRS absorption was masked by PS I absorption in the PS II *T. elongatus* preparation. In this paper, we have had success in accurately quantifying the PS I content at the ~1 mol% level via CD spectroscopy when the PS I present as a contaminant has the same spectral characteristics as that of purified PS I. This process has allowed quantification of the DRS. It has been demonstrated that the absorption characteristics of the PS I red trap region vary depending on whether PS I is in the form of a monomer or trimer [31]. Low temperature CD spectra of monomers and trimers of *T. vulcanus* would be useful, but our ability to quantitatively account

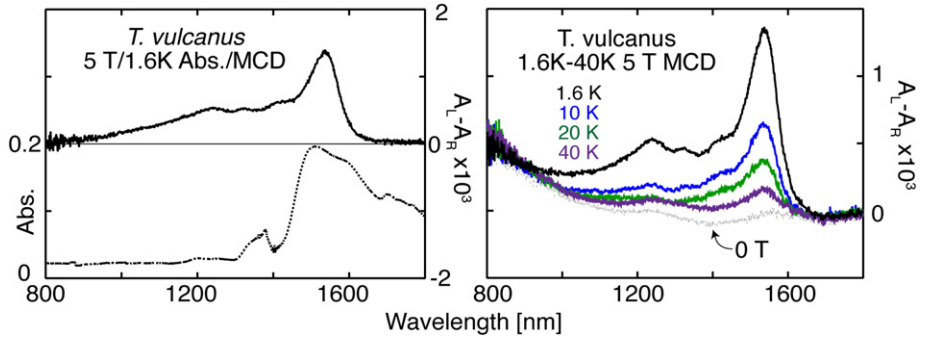

Fig. 7. The left hand panel shows absorption (l.h.scale), MCD (r.h.scale), averaged for positive and negative applied field of 5 T. The r.h. panel shows the temperature dependent MCD in an applied field of 5 T without baseline subtraction. The sample was the same non-recrystallised PS II preparation as used in Fig. 5 but in a 200 μm pathlength cell.

Table 1
Low temperature near-IR absorption and MCD of PS II and PS I.

Organism	Excited state	λ nm	ε M^{-1} cm^{-1}	$(\varepsilon_L - \varepsilon_R)$ M^{-1} cm^{-1} @ 5 T & 1.6 K	$(\varepsilon_L - \varepsilon_R) / \varepsilon$
Spinach					
	PS II Q_y peak	670	2.2×10^6	620	0.0028[a]
	PSII DRS	705	8000	20	~0.002[b]
	PS II Mn(III) S1	770	<30	−5	–
	LMCT cyt b_{559}	1530	–	120	–
	PS I Q_y peak	676	9.8×10^6	–	–
	PS I red trap	710	0.8×10^6	–	–
T. vulcanus					
	PS II Q_y peak	679.5	2.6×10^6	600	0.0023
	PSII DRS	703	8000	16	0.002
	PS II Mn(III) S1	770	<30	−5	>0.1
	LMCT cyt b_{559}	1525	<1000	~250[c]	>0.1
	LMCT cyt c_{550}	1535	–	~250[c]	–
	PS I Q_y peak	679.6	5.5×10^6	1590	0.0029
	PS I red trap	710	0.9×10^6	105	0.0013
	$P700^+$	810	7500[d]	1.8	0.003

ε and $\varepsilon_L - \varepsilon_R$ values are accurate to an estimated ±5–10% (see text).
[a] Ref. [51].
[b] Ref. [22].
[c] See supplementary Fig. S3 and related text.
[d] Ref. [52].

for PS I in PS II cores via CD spectra indicate that PS I is in the same form(s) as in the purified PS I sample.

The data accumulated in Table 1 show that the absorption, CD, MCD characteristics of the DRS in spinach and *T. vulcanus* are essentially the same. Additionally, the efficiency of photoconversion at 720 nm and the 40% drop in intensity of the band upon Q_A^- formation are also the same (Fig. 4). In a recent paper [2] we have shown that both the plant and cyanobacterial samples exhibit a broad emission, originating from the DRS, peaking at 780 nm.

We note that a long-wavelength absorption has been recently proposed [35] for PS I in a number of organisms. It was shown that low temperature excitation at wavelengths far longer than 750 nm leads to PS I charge separation, as evidenced by a bleach of P700 and the creation of $P700^+$. There were other similarities to the DRS state in PS II. The efficiency of the photo-induced process decreased at longer wavelengths, as did the lifetime of the radical produced.

We have seen $P700^+$ creation via 720 nm illumination at 1.6 K (Supplementary Fig. S2B) in a PS I sample of *T. vulcanus*, a result that is consistent with the phenomena reported [35] for *T. elongatus*. It would be possible to apply our non-actinic absorption technique to the near-IR region and quantify the absorption responsible for photochemical activity in PS I, in the same way that has been achieved for PS II.

It has been reported that the DRS in spinach, in marked contrast to Q_y bands of chl-a, does not exhibit spectral hole-burning [22,36–38], as do the lowest energy Q_y states in CP43 and CP47. This was a key result in allowing us to assign the DRS as a homogeneously broadened charge transfer band involving two chl-a's in electronic contact. Similar spectral hole-burning experiments in PS I beyond 742 nm (the limit of red trap Q_y absorption in *T. vulcanus* as shown in Fig. S2B) could also be informative.

It is clear that more theoretical calculations on charge transfer states in photosynthetic systems are warranted. The early theoretical work [39,40] on the closely coupled special pair in the bacterial reaction centre indicated the possibility of optical charge transfer states, but little work seems to have been performed since then.

4.2. Cytochrome charge transfer states

Table 1 summarises the near-IR properties of cyt b_{559} in both spinach and photo-oxidised cyt b_{559} in *T. vulcanus*, as well as that of cyt c_{550} in *T. vulcanus*. The MCD is characteristic of the LMCT excitation associated with electron transfer from the cytochrome heme to low spin Fe(III). The MCD peaks near 1530 nm but extends to ~800 nm. The recognition of the high energy reach of the LMCT band(s) has been critical in the identification of Mn(III)-based MCD in the 730–850 nm region.

Oxidised cytochrome MCD signals are stronger in *T. vulcanus* than in spinach for a number of reasons. Firstly, cyt c_{550} is oxidised in the native *T. vulcanus* preparation and thus will always appear in the near-IR MCD. Secondly, although cyt b_{559} is largely reduced in the best PS II core preparations, the MCD of (photo)-oxidised *T. vulcanus* cyt b_{559} is more than twice as strong as that for oxidised cyt b_{559} in spinach (Table 1). Also LMCT bands in *T. vulcanus* are slightly blue shifted (Table 1) compared to the (fully oxidised) cyt b_{559} present in spinach PS II core complexes and thus serve to interfere with the Mn(III) signals more effectively.

Measurements of the near-IR MCD characteristics of oxidised cytochromes are a natural partner to EPR spectroscopies. MCD measurements can clearly be used to further study the various (high-potential, low-potential forms [41]) of oxidised cytochromes in PS II, as the signals are strong and the methodologies well established. However in this study, the main focus is to identify Mn(III)-based excitations of the Mn_4CaO_5 cluster.

4.3. Quantification and assignment of near-IR Mn(III) states

The identification of optical absorptions in the 700–900 nm range that give rise to Mn_4CaO_5 based photochemistry in PS II has been a long-standing challenge, largely due to the low absorption strength of the transitions involved. It is now evident that Mn(III)-related absorptions are bounded by DRS absorption to higher energies and oxidised cytochrome absorptions to lower energies. Additionally, PS I present in PS II preparations also interfere.

The MCD technique offers a way to both detect weak Mn(III)-related transitions and also to discriminate between the various excitations present in the near-IR. We have been able to identify MCD *B* terms associated with the DRS and Q_y excitations of contaminating PS I in the 700–740 nm region as well as MCD *C* terms associated with LMCT excitations of oxidised cytochromes in the 800–1600 nm region.

Figs. 5 and 6 serve to show that MCD here has a continually varying behaviour throughout in the 700–900 nm region. The 860–900 nm region is dominated by cytochrome LMCT transitions. The precise form of the saturation behaviour [21] for an oxidised cytochrome, which is an anisotropic odd electron paramagnet, depends on its g_x, g_y and g_z values and additionally on the magnitude and relative orientation of the anisotropic transition dipoles involved. This dependence on the transition moments means that different optical transitions of the same cytochrome display different saturation curves [20].

A precise measurement of LMCT saturation behaviour could be more easily made at the peak of the MCD (near 1530 nm), as the MCD signal is much stronger there and thus less prone to the type of offset difficulties mentioned in previous sections. However the precise form of MCD saturation behaviour determined at the 1530 peak of *T. vulcanus* may not be fully transferrable to the 860–900 nm region as a cytochrome LMCT band is itself composite [42] of excitations involving two different heme orbitals. Additionally the relative contribution of cyt c_{550} and cyt b_{559} differ at differing wavelengths (Fig. S3, Table 1).

The temperature and magnetic field dependence of the MCD near 770 nm is clearly complex and distinct to that seen for the 860–900 nm region. The behaviour points to the highly variable MCD saturation behaviour exhibited by even electron paramagnets [14]. There is a sharp drop of MCD at higher temperatures, exceeding the *C* term 1/Temperature behaviour exhibited by the cytochromes. In some situations for an even electron paramagnet, an increasing magnetic field can lead to a decrease in MCD intensity. Additionally, the four Mn(II)/Mn(III)/Mn(IV) centres present in the OEC are magnetically coupled, as evidenced by EPR spectroscopies [43–45]. MCD spectra are

significantly influenced by such couplings [46]. These dependencies point to the potential of near-IR MCD providing a new window on the nature of the OEC.

4.4. Alternative assignments

The possibility that the 770 nm MCD feature seen is due to a Mn(III)-Mn(IV) mixed valence excitation is contraindicated by the large $\varepsilon_L - \varepsilon_R / \varepsilon$ exhibited by the band, as well as its relatively narrow bandwidth. Mixed-valence transitions are characteristically linearly polarised, which leads to vanishingly small MCD [13]. By contrast, d–d transitions have inherently large values of $\varepsilon_L - \varepsilon_R / \varepsilon$.

Based on the established relationship between the spectral width of a localised homo-nuclear mixed-valence band and its band position [47], a mixed-valence band at 770 nm would be approximately 5500 cm^{-1} wide whereas the observed linewidth is closer to 500 cm^{-1}.

There are two further paramagnetic species in PS II which could potentially contribute to temperature dependent MCD in the near-IR region. Firstly, the non-heme iron of PS II is an effectively octahedral [48] Fe(II) species with a high-spin d^4 configuration. This will exhibit a spin-allowed 10Dq band in the near-IR region. The detailed study [49] of a range of non-heme Fe(II) species has shown that their MCD is weak and positive (~1 M^{-1} cm^{-1} at 5 T and 1.6 K), peaking near 800 nm for octahedral species. Thus the non-heme Fe(II) in PS II is not responsible for the stronger (and negative) MCD near 770 nm, but may be associated with weaker MCD features near 800 nm.

Additionally, it has been suggested [50] that a d–d transition of an unusual, highly distorted Mn(IV) species may be responsible for the absorption associated with near-IR induced photo-activity seen in EPR spectra of the S_3 state. Whilst not immediately relevant to our measurements taken with the S_1 state, near-IR MCD measurements of PS II poised in the S_3 state promise to provide a more definitive assignment of the chromophore responsible for this photo-activity.

4.5. Future developments

At this stage, a quantitative analysis of the data and subsequent modelling of the Mn(III) geometries and magnetic couplings within the Mn_4CaO_5 cluster, via an analysis of the MCD and its field and temperature dependence is not viable, not so much now by absolute sensitivity issues, but by the offset problem associated with minute magnet energization-induced sample movement discussed in previous sections. This problem is currently being addressed by re-engineering the magnet cryostat enclosure using non-magnetic materials and with improvements to the optics.

Our experiments are reported for the S_1Q_A dark-adapted state of PS II. It is important to be able to compare these measurements with those made in the higher S states, as well as their related near-IR illuminated variants. We have attempted to make measurements on PS II poised in the $S_2Q_A^-$ state, as created by illumination of the sample at 250–270 K via illumination with green light from a halogen lamp. These experiments did show a reduction in MCD in the 770 nm region but the experiment was hampered by fogging of the sample that occurred when warming the sample to these temperatures. The cloudiness of the sample not only dramatically reduced transmission of the sample also served to depolarise the incident measurement light.

It is preferable to create PS II core samples poised in the higher S states by using saturating 5 ns laser pulses at 532 nm at ambient temperatures, followed by rapid freezing of the sample. Our thick, concentrated samples have high optical density at 532 nm and a high energy (>200 mJ) pulse(s) is/are required to provide a satisfactory yield of a higher S state(s). This requires an upgrade of our current YAG laser. An illumination system that enables the conversion an optical sample to higher S states via high-energy YAG pulses, whilst securing the optical cell in the dry helium environment of the sample lock of the superconducting magnet cryostat is also being constructed.

We envisage being able to generate a set of accurate field and temperature dependent MCD spectra for each sample. These can then be used to construct a saturation curves for each wavelength region. An analysis of this family of saturation curves will then indicate the contribution at each wavelength of chl-a/Mn(III)/Fe(II)/cytochrome excitations. The MCD of each Mn(III) MCD in each S state can then be modelled to provide information on its geometry, ligation and magnetic coupling within the $CaMn_4O_5$ cluster.

5. Conclusions

We have shown that the properties of the DRS absorption as seen in the 700–730 nm region are essentially the same in spinach and *T. vulcanus*. Consequently, the DRS is likely to be similar in most plants and cyanobacteria. With the very recently reported [35] phenomenon of a similar charge transfer band in PS I, the function as well as significance of low energy charge transfer states in oxygenic photosynthesis needs to be addressed, both theoretically and experimentally.

The LMCT transitions of oxidised cytochromes in PS II have been identified and quantified, via their MCD spectra, as extending through the entire 800–1600 nm region. Most interestingly, the optical signature of an Mn(III)-based absorption near 770 nm has been identified via low temperature MCD. A corresponding absorption in this region is estimated to have a molar extinction less than ~30 M^{-1} cm^{-1}. On the basis of the low absorption strength and the relatively high MCD strength of −5 M^{-1} cm^{-1} at 1.6 K and 5 T, the transition is assigned as a $d_z^2 \rightarrow d_{x2-y2}$ process, in analogy to a comparable low energy feature in oxidised manganese catalase [15].

Acknowledgements

We would like to dedicate this paper to our late colleague Warwick Hillier whose untimely death was a shock to his friends and colleagues. He was involved in the early stages of this project. The tireless technical support of Keith Jackman was critical in many aspects of this demanding project. Paul Smith prepared the spinach PS II core complexes used in this work. We would like to acknowledge the continuing help and encouragement of Bill Rutherford and Nick Cox. We recognise the support of the Australian Research Council through grant DP110104565 (E.K.) and MEXT/JSPS of Japan through a Grant-in-Aid for Specially Promoted Research No. 24000018 (J.R.S.).

Appendix A. Supplementary data

Supplementary data to this article can be found online at http://dx.doi.org/10.1016/j.bbabio.2014.11.003.

References

[1] J.L. Hughes, P. Smith, R. Pace, E. Krausz, Charge separation in photosystem II core complexes induced by 690–730 nm excitation at 1.7 K, Biochim. Biophys. Acta 1757 (2006) 841–851.
[2] J. Morton, J. Hall, P. Smith, A. Fusamichi, F. Koua, J.-R. Shen, E. Krausz, Determination of the PS I content of PS II core preparations using selective emission: a new emission of PS II at 780 nm, Biochim. Biophys. Acta Bioenerg. 1837 (2014) 167–177.
[3] O. Nanba, K. Satoh, Isolation of a photosystem ii reaction center consisting of D-1 and D-2 polypeptides and cytochrome *b*-559, Proc. Natl. Acad. Sci. 84 (1987) 109–112.
[4] E. Krausz, N. Cox, S.P. Arskold, Spectral characteristics of PS II reaction centres: as isolated preparations and when integral to PS II core complexes, Photosynth. Res. 98 (2008) 207–217.
[5] Y. Umena, K. Kawakami, J.R. Shen, N. Kamiya, Crystal structure of oxygen-evolving photosystem II at a resolution of 1.9 angstrom, Nature 473 (2011) 55–60.
[6] A. Boussac, J.J. Girerd, A.W. Rutherford, Conversion of the spin state of the manganese complex in photosystem II induced by near-infrared light, Biochemistry 35 (1996) 6984–6989.
[7] A. Boussac, M. Sugiura, D. Kirilovsky, A.W. Rutherford, Near-infrared-induced transitions in the manganese cluster of photosystem II: action spectra for the S-2 and S-3 redox states, Plant Cell Physiol. 46 (2005) 837–842.

[8] A. Cua, D.H. Stewart, M.J. Reifler, G.W. Brudvig, D.F. Bocian, Low-frequency resonance Raman characterization of the oxygen-evolving complex of photosystem II, J. Am. Chem. Soc. 122 (2000) 2069–2077.
[9] G.C. Dismukes, P. Mathis, A near infrared electronic transition associated with conversion between S-states of the photosynthetic O_2-evolving complex, FEBS Lett. 178 (1984) 51–54.
[10] B.R. Velthuys, Spectroscopic characterization of the acceptor state Qa- and the donor state-S2 of photosystem-Ii of spinach in the blue, red and near-infrared, Biochim. Biophys. Acta 933 (1988) 249–257.
[11] R. Baxter, E. Krausz, T. Wydrzynski, R.J. Pace, Identification of the near-infrared absorption band from the Mn cluster of photosystem II, J. Am. Chem. Soc. 121 (1999) 9451–9452.
[12] R. Steffen, K. Jackman, E. Krausz, Design and application of a high-precision, broad spectral range CCD-based absorption spectrometer with millisecond time resolution, Meas. Sci. Technol. 19 (2008).
[13] S.B. Piepho, P.N. Schatz, Group Theory in Spectroscopy With Applications to Magnetic Circular Dichroism, Wiley-Interscience, New York, Chichester, Brisbane, Toronto, Singapore, 1983.
[14] E.I. Solomon, E.G. Pavel, K.E. Locb, C. Campochiaro, Magnetic circular dichroism spectroscopy as a probe of the geometric and electronic structure of non-heme ferrous enzymes, Coord. Chem. Rev. 144 (1995) 369–460.
[15] T.C. Brunold, D.R. Gamelin, T.L. Stemmler, S.K. Mandal, W.H. Armstrong, J.E. Penner-Hahn, E.I. Solomon, Spectroscopic studies of oxidized manganese catalase and mu-oxo-bridged dimanganese(III) model complexes: electronic structure of the active site and its relation to catalysis, J. Am. Chem. Soc. 120 (1998) 8724–8738.
[16] A.J. Wu, J.E. Penner-Hahn, V.L. Pecoraro, Structural, spectroscopic, and reactivity models for the manganese catalases, Chem. Rev. 104 (2004) 903–938.
[17] D.R. Gamelin, M.L. Kirk, T.L. Stemmler, S. Pal, W.H. Armstrong, J.E. Pennerhahn, E.I. Solomon, Electronic-structure and spectroscopy of manganese catalase and Di–Mu–Oxo [Mn(III)Mn(IV)] model complexes, J. Am. Chem. Soc. 116 (1994) 2392–2399.
[18] R.A. Geiger, D.F. Leto, S. Chattopadhyay, P. Dorlet, E. Anxolabehere-Mallart, T.A. Jackson, Geometric and electronic structures of peroxomanganese(III) complexes supported by pentadentate amino-pyridine and -imidazole ligands, Inorg. Chem. 50 (2011) 10190–10203.
[19] C. Houssier, K. Sauer, Circular dichriosm and magnetic circular dichroism of the chlorophyll and protochlorophyll pigments, J. Am. Chem. Soc. 92 (1970) 779–791.
[20] M.R. Cheesman, C. Greenwood, A.J. Thomson, Magnetic circular-dichroism of hemoproteins, Adv. Inorg. Chem. Rad. 36 (1991) 201–255.
[21] P.N. Schatz, R.L. Mowery, E.R. Krausz, MCD/MCPL [magnetic CD/magnetic circularly polarized luminescence] saturation theory with application to molecules in Dh and its subgroups, Mol. Phys. 35 (1978) 1537–1557.
[22] E. Krausz, J.L. Hughes, P. Smith, R. Pace, S. Peterson Årsköld, Oxygen-evolving photosystem II core complexes: a new paradigm based on the spectral identification of the charge-separating state, the primary acceptor and assignment of low-temperature fluorescence, Photochem. Photobiol. Sci. 4 (2005) 744–753.
[23] R. Stranger, L. Dubicki, E. Krausz, Magneto-optical investigation of the exchange-coupled dimer $Cs_3Mo_2Br_9$, Inorg. Chem. 35 (1996) 4218–4226.
[24] E. Krausz, Selective and differential optical spectroscopies in photosynthesis, Photosynth. Res. 116 (2013) 411–426.
[25] J.L. Hughes, E. Krausz, Electronic spectroscopy, in: R.A. Scott, C.M. Lukehart (Eds.), Application of Physical Methods to Inorganic and Bioinorganic Chemistry, John Wiley & Sons, Ltd., 2007
[26] J.R. Shen, Y. Inoue, Binding and functional properties of two new extrinsic components, cytochrome c-550 and a 12-kDa protein, in cyanobacterial photosystem II, Biochemistry 32 (1993) 1825–1832.
[27] J.R. Shen, N. Kamiya, Crystallization and the crystal properties of the oxygen-evolving photosystem II from *Synechococcus vulcanus*, Biochemistry 39 (2000) 14739–14744.
[28] H. Matsuoka, K. Furukawa, T. Kato, H. Mino, J.R. Shen, A. Kawamori, Anisotropy of the S-2-state manganese cluster in single crystals of cyanobacterial photosystem II studied by W-band electron paramagnetic resonance spectroscopy, J. Phys. Chem. B 110 (2006) 13242–13247.
[29] W.L. Butler, S. Okayama, The photoreduction of C-550 in chloroplasts and its inhibition by lipase, Biochim. Biophys. Acta 245 (1971) 237–239.
[30] E. Krausz, A single-beam approach to the absorption spectroscopy of microcrystals, Aust. J. Chem. 46 (1993) 1041–1054.
[31] E. Schlodder, M. Hussels, M. Cetin, N.V. Karapetyan, M. Brecht, Fluorescence of the various red antenna states in photosystem I complexes from cyanobacteria is affected differently by the redox state of P700, Biochim. Biophys. Acta Bioenerg. 1807 (2011) 1423–1431.
[32] J.L. Hughes, P.J. Smith, R.J. Pace, E. Krausz, Low energy absorption and luminescence of higher plant photosystem II core samples, J. Lumin. 122–123 (2007) 284–287.
[33] A.J. Thomson, D.G. Englinton, B.C. Hill, C. Greenwood, The nature of Haem-A3 in the oxidized state of cytochrome-C oxidase — evidence from low-temperature magnetic-circular-dichroism spectroscopy in the near-infrared region, Biochem. J. 207 (1982) 167–170.
[34] J.L. Hughes, N. Cox, A.W. Rutherford, E. Krausz, T.L. Lai, A. Boussac, M. Sugiura, D1 protein variants in photosystem II from *Thermosynechococcus elongatus* studied by low temperature optical spectroscopy, Biochim. Biophys. Acta Bioenerg. 1797 (2010) 11–19.
[35] E. Schlodder, F. Lendzian, J. Meyer, M. Cetin, M. Brecht, T. Renger, N.V. Karapetyan, Long-wavelength limit of photochemical energy conversion in photosystem I, J. Am. Chem. Soc. 136 (2014) 3904–3918.
[36] J.L. Hughes, E. Krausz, Novel characteristics of persistent spectral hole-burning and hole-filling in photosystem II core complexes, J. Lumin. 127 (2007) 239–244.
[37] J.L. Hughes, P.J. Smith, R.J. Pace, E. Krausz, Spectral hole burning at the low-energy absorption edge of photosystem II core complexes, J. Lumin. 119–120 (2006) 298–303.
[38] J.L. Hughes, B.J. Prince, E. Krausz, P.J. Smith, R.J. Pace, H. Riesen, Highly efficient spectral hole-burning in oxygen-evolving photosystem II preparations, J. Phys. Chem. B 108 (2004) 10428–10439.
[39] A. Warshel, W.W. Parson, Spectroscopic properties of photosynthetic reaction centres. 1. Theory, J. Am. Chem. Soc. 109 (1987) 6143–6152.
[40] W.W. Parson, A. Warshel, Spectroscopic properties of photosynthetic reaction centres. 2. Application of the theory to *Rhodopseudomonas viridis*, J. Am. Chem. Soc. 109 (1987) 6152–6163.
[41] D.H. Stewart, G.W. Brudvig, Cytochrome b559 of photosystem II, Biochim. Biophys. Acta 1367 (1998) 63–87.
[42] A. Schejter, W.A. Eaton, Charge-transfer optical-spectra, electron-paramagnetic resonance, and redox potentials of cytochromes, Biochemistry 23 (1984) 1081–1084.
[43] D.A. Pantazis, W. Ames, N. Cox, W. Lubitz, F. Neese, Two interconvertible structures that explain the spectroscopic properties of the oxygen-evolving complex of photosystem II in the S2 state, Angew. Chem. Int. Edit. 51 (2012) 9935–9940.
[44] S.L. Dexheimer, M.P. Klein, Detection of a paramagnetic intermediate in the S1-state of the photosynthetic oxygen-evolving complex, J. Am. Chem. Soc. 114 (1992) 2821–2826.
[45] T. Yamauchi, H. Mino, T. Matsukawa, A. Kawamori, T. Ono, Parallel polarization electron paramagnetic resonance studies of the S-1-state manganese cluster in the photosynthetic oxygen-evolving system, Biochemistry 36 (1997) 7520–7526.
[46] T.C. Brunold, D.R. Gamelin, E.I. Solomon, Excited-state exchange coupling in bent Mn(III)-O-Mn(III) complexes: dominance of the pi/sigma superexchange pathway and its possible contributions to the reactivities of binuclear metalloproteins, J. Am. Chem. Soc. 122 (2000) 8511–8523.
[47] S.B. Piepho, E.R. Krausz, P.N. Schatz, Vibronic coupling model for calculation of mixed-valence absorption profiles, J. Am. Chem. Soc. 100 (1978) 2996–3005.
[48] N. Cox, L. Jin, A. Jaszewski, P.J. Smith, E. Krausz, A.W. Rutherford, R. Pace, The semiquinone-iron complex of photosystem II: structural insights from ESR and theoretical simulation; evidence that the native ligand to the non-heme iron is carbonate, Biophys. J. 97 (2009) 2024–2033.
[49] E.I. Solomon, A. Decker, N. Lehnert, Non-heme iron enzymes: contrasts to heme catalysis, Proc. Natl. Acad. Sci. U. S. A. 100 (2003) 3589–3594.
[50] N. Cox, M. Retegan, F. Neese, D.A. Pantazis, A. Boussac, W. Lubitz, Photosynthesis. Electronic structure of the oxygen-evolving complex in photosystem II prior to O–O bond formation, Science 345 (2014) 804–808.
[51] P.J. Smith, S. Peterson, V.M. Masters, T. Wydrzynski, S. Styring, E. Krausz, R.J. Pace, Magneto-optical measurements of the pigments in fully active photosystem II core complexes from plants, Biochemistry 41 (2002) 1981–1989.
[52] P. Mathis, P. Setif, Near-infrared absorption-spectra of the chlorophyll-a cations and triplet-state in vitro and in vivo, Isr. J. Chem. 21 (1981) 316–320.